Polymer-Protected Ni/Pd Bimetallic Nano-Clusters: Preparation, Characterization and Catalysis for Hydrogenation of Nitrobenzene

Ping Lu,[†] Toshiharu Teranishi,[‡] Kiyotaka Asakura,[§] Mikio Miyake,[‡] and Naoki Toshima*[,||]

Department of Applied Chemistry, School of Engineering, The University of Tokyo, Hongo, Bunkyo-ku, Tokyo 113-8656, Japan, School of Materials Science, Japan Advanced Institute of Science and Technology, 1-1 Asahidai, Tatsunokuchi, Nomi-gun, Ishikawa 923-1292, Japan, Department of Chemistry, School of Science, The University of Tokyo, Hongo, Bunkyo-ku, Tokyo 113-8656, Japan, and Department of Materials Science and Engineering, Science University of Tokyo in Yamaguchi, Onoda-shi, Yamaguchi 756-0884, Japan

Received: June 28, 1999; In Final Form: August 18, 1999

Well-dispersed and stable colloidal dispersions of polymer-protected Ni/Pd bimetallic nanoclusters have been obtained over an entire composition range by an improved polyol reduction method, in which nickel(II) sulfate and palladium(II) acetate were reduced at high temperature by ethylene glycol in the presence of poly(*N*-vinyl-2-pyrrolidone). Transmission electron microscopy indicates that these bimetallic nanocluster particles have definitely monodispersed size-distributions, with each particle containing both nickel and palladium atoms. The alloy structure has also been shown by X-ray diffraction and extended X-ray absorption fine-structure analysis. X-ray absorption near-edge spectroscopic and X-ray photoelectron spectroscopic data have confirmed that the nickel in the bimetallic nanoclusters is in the zero-valence state, as stabilized by the presence of Pd. Dispersions of these bimetallic nanoclusters were used as homogeneous catalysts for hydrogenation of nitrobenzene at 30 °C under an atmospheric pressure of hydrogen. The catalytic activities are demonstrated to be dependent on the metal composition of the particles. The highest activity can be achieved for a bimetallic nanocluster with a molar ratio of Ni:Pd = 2:3, which exhibits 3.5 times greater activity than that of a typical colloidal palladium catalyst.

1. Introduction

Bimetallic alloy nanoclusters have received increasing attention in the past 20 years especially as catalysts since the addition of the second metal provides a method of controlling the activity, selectivity, and stability of the catalysts in certain reactions.[1] In the bimetallic catalysts supported on high-surface-area refractories, i.e., the fine particles dispersed on inorganic oxide supports such as Al_2O_3, SiO_2, TiO_2, and MgO, the shape, size, and composition of metal particles as well as the interactions with supports have been studied to explore the properties of metal nanoclusters.[2] Several factors may affect the compositions and structure of bimetallic particles, including the bulk immiscibility of each component in a phase diagram.[3] Colloidal dispersions of metal nanoclusters protected by polymers in a homogeneous solution bear an obvious advantage of their high degree of dispersion. Since the interaction of metal nanoclusters with a protective macromolecule is not so strong as that of metal nanoclusters with a support in supported metal catalysts, colloidal dispersions of noble-metal nanoclusters could be expected to provide a favorable system for investigation of the surface structure of metal nanoclusters. Consequently, much attention has been paid to polymer-protected bimetallic nanoclusters composed of two kinds of noble metals. Richard et al. used transmission electron microscopy (TEM), X-ray absorption spectroscopy (XAS), and X-ray scattering techniques to characterize the colloidal Pt/Ru particles, and showed that an added Ru surface layer in the bimetallic nanoclusters reduces the number of unoccupied d-states in the Pt fcc core and has a moderate effect on the catalytic selectivity as the result of changes in electronic properties.[4] We have reported in a series of papers that the colloidal dispersions of bimetallic nanoclusters (Au/Pd, Pt/Rh, Pd/Rh, Pd/Pt, etc.) can be prepared by reducing two kinds of noble-metal ions with alcohols in the presence of poly(*N*-vinyl-2-pyrrolidone) (PVP).[5−12] These bimetallic nanoclusters keeping the composition of charged mole ratio of the metals in each alloy particle were shown to have a size distribution of 2−7 nm and a tendency to form a core/shell structure. Thus, one kind of metal is located mainly on the particle surface, forming a shell, and the other metal, near the center of the particle forming a core, which has been revealed by extended X-ray absorption fine structure (EXAFS) analysis, infrared spectroscopy, X-ray photoelectron spectroscopy (XPS), and so on.[5−8] The redox potentials of metal ions and coordination ability of metal to polymer ligands are considered as the main factors to control the core/shell structure.[9,10]

Bimetallic clusters composed of a noble metal and a light transition metal should be prospective with their high potential in tailoring the structures and the catalytic properties. Bradley et al. reported the preparation of Cu/Pd colloids by thermal decomposition of mixtures of the corresponding metal acetates in the presence of polymeric protective agents,[13,14] and showed the 0-valency of Cu on the alloy particles by IR spectra of the CO molecules adsorbed on Cu. Independently we have demonstrated that both Cu/Pt and Cu/Pd nanoclusters with various

* Corresponding author. Telephone: +81-836-88-4561. Fax: +81-836-88-4567. E-mail: toshima@ed.yama.sut.ac.jp.

[†] Department of Applied Chemistry, School of Engineering, The University of Tokyo.

[‡] School of Materials Science, Japan Advanced Institute of Science and Technology.

[§] Department of Chemistry, School of Science, The University of Tokyo.

[||] Department of Materials Science and Engineering, Science University of Tokyo in Yamaguchi.

10.1021/jp992177p CCC: $18.00
Published on Web 10/16/1999

Cu/noble metal mole ratios even higher than one, can be prepared by alcoholic reduction at high temperature, resulting in alloy particles with average diameters of only 1−3 nm.[15] Unlike binary noble metal nanoclusters, the Cu/Pt nanoclusters, thus prepared, no longer have the core/shell structure, but instead possess structures similar to bulk CuPt or Cu_3Pt, depending on the feed mole ratio. The Cu/Pd nanoclusters can serve as excellent catalysts for both selective partial hydrogenation of 1,3-cyclooctadiene to cyclooctene and selective hydration of acrylonitrile to acrylamide. The Cu-containing nanoclusters protected by PVP may also exhibit controllable nonlinear optical properties inherited from monometallic Cu particles protected by PVP, which were pointed out recently.[16]

In comparison with Cu-containing alloy particles, preparation of Ni-containing noble-metal nanoclusters is expected to be difficult, since the reduction potential of Ni(II) ion is more negative than that of Cu(II) (E^0 (Ni^{2+}/Ni^0) = −0.257 V and E^0 (Cu^{2+}/Cu^0) = 0.342 V vs NHE). However, Ni-containing nanoparticles are one of the interesting materials for advanced technologies. Very recent studies, for example, show that PVP-protected bilayered Ni/Pd nanoclusters have enhanced magnetic susceptibility at low temperatures due to quantum size effect.[17] Thus this type of nanoscopic alloys (Pd/ferromagnetic metals) represents a new class of materials whose catalytic and physical properties should be characterized and explored to understand their uniqueness. Actually, little is known about the central question of the electronic structures of bimetallic clusters of groups 8−10. Since both Ni and Pd belong to the same group 10 in the periodic table, the interactions (mixing) between Ni $3d^84s^2$ electrons and Pd $4d^{10}5s^0$ electrons are very likely involved in intermetallic Ni−Pd bonding. Such effect on the catalysis by nanometer-sized Ni/Pd clusters is certainly interesting. In this paper, the preparation and characterization of a novel PVP-protected Ni/Pd bimetallic nanoclusters and their catalysis for hydrogenation of nitrobenzene are reported.

2. Experimental Section

Materials. PVP (K-30, average molecular weight 40 000) was purchased from Tokyo Kasei. Co., Ltd. Other reagents, nickel sulfate ($NiSO_4 \cdot 7H_2O$), palladium(II) acetate ($Pd(Ac)_2$), dioxane, sodium hydroxide, glycol, Raney nickel precursor, and palladium black, each having a purity level higher than GR grade, were used without further purification. Nitrobenzene was distilled before use.

Preparation of Colloidal Dispersions of Ni/Pd Bimetallic Nanoclusters. The colloidal dispersions of the Ni/Pd bimetallic nanoclusters protected by polymers were prepared by an improved polyol reduction method. Palladium(II) acetate and nickel(II) sulfate were used as the starting materials since they have reasonably good solubility in the organic solvents. Palladium(II) acetate was dissolved in dioxane (15.6 mM $Pd(Ac)_2$) and stirred for 1 day, resulting in a clear yellow solution. In a 1000-mL three-neck flask, PVP (4.006 g, 35.7 mmol in monomeric units, 14.3 times the total amount of metal ions in moles) and nickel(II) sulfate ($NiSO_4 \cdot 7H_2O$) were dissolved in 600 mL of glycol at 80 °C. To this solution, the dioxane solution of $Pd(Ac)_2$ was added at 0−5 °C, and pH values were adjusted to 9−11 by dropwise addition of an aqueous solution of sodium hydroxide (NaOH, 1 M). Two metal ions were mixed at designated mole ratios and the total amount of the metal ions was always kept constant at 2.5 mmol. The solutions were stirred and refluxed at 198 °C for 3 h with a nitrogen flow passing through the reaction system to take away water and organic byproducts. The color of the mixed solution suddenly changed from clear yellow to transparent dark brown at the initial stage of the refluxing. The final colloidal dispersions appeared as transparent dark-brown homogeneous solutions and were rather stable. PVP-protected monometallic nickel and palladium colloidal dispersions were also obtained by a similar procedure. In the case of PVP-protected nickel nanoclusters, the amount of PVP was increased by 4 times, and a mechanical stirring rod was utilized so as to overcome the strong magnetic attraction force in the nickel metal which would otherwise enhance the tendency of coagulation and precipitation of the nickel nanoparticles.

Characterization of the Ni/Pd Bimetallic Nanoclusters. Samples for TEM measurements were prepared by placing a drop of the colloidal dispersions of metal nanoclusters onto a carbon-coated copper micro-grid (kindly provided by Dr. K. Adachi, the University of Tokyo), transferring most of the solvents onto a filter paper by capillary action, and then drying under vacuum for 1 day. TEM photographs were taken at 125 kV acceleration voltage on a Hitachi H-7100 electron microscope. The mean diameter and standard deviation were calculated by counting 200 particles from the TEM photograph of 400 000 magnifications by using a magnifier (10×). High-resolution transmission electron microscopy (HRTEM) measurements were carried out on a Hitachi H-9000NAR electron microscope at 300 kV.

Samples for X-ray diffraction (XRD) measurements were prepared by vacuum evaporation of glycol from the nanocluster dispersion with a large dry ice freezing trap for glycol solvent and by drying the residual glycol under vacuum for a day. Evaporation and drying were carried out at a temperature as low as possible to prevent any structural change of metal nanocluster. XRD patterns were recorded on a Rigaku Rint 2400 diffractometer with Cu Kα radiation (λ = 1.54050 Å) at 40 kV and 200 mA. Continuous X-ray scans were carried out from 2θ of 30° to 90° with a step width of 0.01° and a counting time of 2.4 s.

XPS data were measured with a Kratos AXIS-HS spectrometer. The Mg Kα X-ray line (1253.6 eV) was used for photoelectron excitation. All spectra were referenced to the C1s photoelectron peak of 284.6 eV. The same method as that for XRD was employed for XPS sample preparation.

Ni K-edge X-ray absorption near-edge structure (XANES) as well as Ni K-edge and Pd K-edge EXAFS measurements were carried out in a transmission mode at the BL-7C (Ni−K) and BL-10B (Pd−K) beamlines of Photon Factory, the National Laboratory for High Energy Physics (KEK-PF) at Tsukuba, Japan, using synchrotron radiation at room temperature. The channel-cut Si(111) (Ni−K) and Si(311) (Pd−K) monochromators were used. The storage ring was operated at 3.0 (Ni−K) and 2.5 (Pd−K) GeV, and the ring current was in the range of 100−300 mA. The colloidal samples for the XAS measurements were concentrated by ultra-filtration and the concentrated dispersions were put in a glass sample cell with polyimide windows under nitrogen atmosphere. The cells with optical path lengths of 5−10 and 50 mm were used for Ni K-edge and Pd K-edge measurements, respectively. The reference compounds used were monometallic Ni and Pd metal foils, and bimetallic Ni/Pd(9/1, mole ratio), Ni/Pd(1/1), and Ni/Pd(1/9) alloy foils, produced by Tanaka Kikinzoku Kogyo K. K. in accordance with our request, as well as NiO and Ni_3O_4 prepared as finely ground powders and fixed on adhesive Kapton tapes.

As for the contribution of the metal−metal bonds, Fourier transformation of $k^3\chi(k)$ was carried out over the region 30−160 nm^{-1}. The peak in the Fourier transform was filtered over

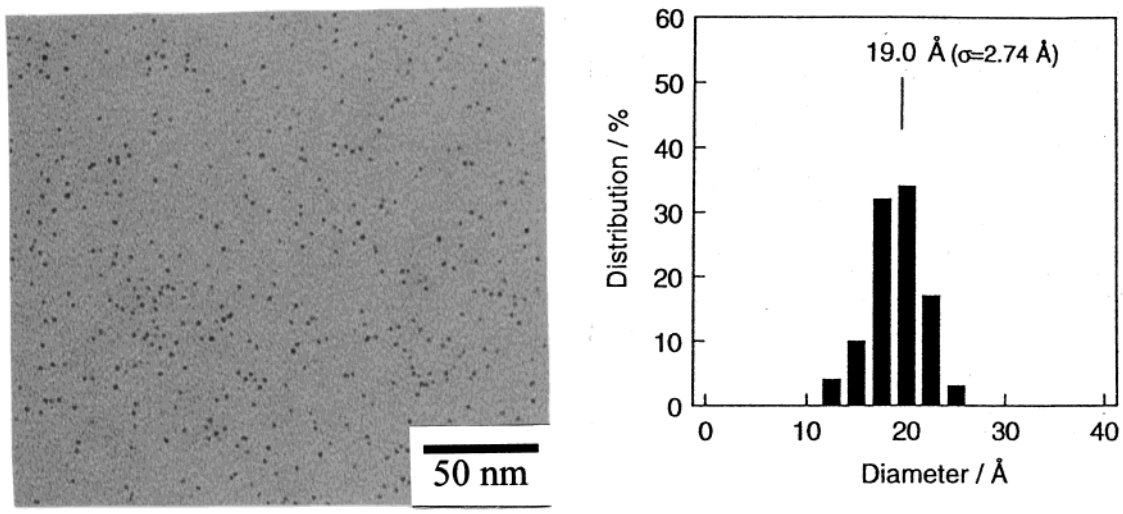

Figure 1. TEM micrograph and size distribution of Ni/Pd(2/3) nanoclusters: $d_{av} = 1.9$ nm, $\sigma = 0.27$ nm.

0.15−0.30 nm and inversely Fourier transformed into *k*-space (the region 40−150 nm^{-1}) again. The Fourier-filtered data were then analyzed with a curve-fitting technique,[5−8] by using the REX program developed by Rigaku Co.

Hydrogenation of Nitrobenzene. The hydrogenation of nitrobenzene was carried out in ethanol at 30.0 °C under hydrogen at an atmospheric pressure. The polymer-protected Ni/Pd bimetallic nanoclusters were dried by the same method as described above for the XRD samples. The desired amount of the dried polymer-protected bimetallic nanoclusters was then dispersed again into a calculated amount of ethanol to form a 0.1 mM ethanol dispersion of metal nanoclusters as catalysts. W-6 Raney nickel catalysts were prepared in the conventional method as reported in the references.[18,19] W-6 Raney nickel, along with palladium black, was also made into a 0.1 mM ethanol dispersion for use as catalysts. The catalyst dispersion (20 mL, total metal = 2×10^{-6} mol) was injected into a 50 mL flask, where the air was thoroughly exchanged in advance by hydrogen at one atmospheric pressure. The solution containing the catalyst was stirred at 30.0 °C to activate the catalyst. After the initial hydrogenation uptake ceased, 1.0 mL of ethanol solution containing 0.3 mmol of nitrobenzene was added to the flask keeping the total pressure at 1 atm. The progress of hydrogenation was followed by hydrogen uptake with a temperature-controlled gas buret. The initial rate, determined by the initial slope of hydrogen uptake (cf. inset of Figure 8), was used for the evaluation of catalytic activity in this paper.

The hydrogenation products were analyzed with a Shimadzu GC-14B capillary gas chromatography using a 25m × 0.25 mmØ WCOT fused silica capillary column.

3. Results and Discussion

Preparation and Characterization of Colloidal Dispersions of the Ni/Pd Bimetallic Nanoclusters. Colloidal dispersions of Ni/Pd bimetallic nanoclusters were successfully prepared by glycol reduction at high temperature in the presence of PVP, which appeared as clear dark-brown solutions and had good anti-oxidation properties. They are stable for months under nitrogen at room temperature. Especially, the very dilute (0.1 mM) colloidal dispersions of the bimetallic nanoclusters, made for the use of catalysis, showed neither precipitates nor inferiority in catalytic activities even after being kept for half a year. The high stability may be caused by complete surrounding of nanoclusters by polymer and keeping nanoclusters in a glycol solution, i.e., reductive medium.[10]

Transmission electron micrograph (TEM) was measured to characterize the nanoclusters. Particularly fine and well-shaped bimetallic nanoparticles with narrow size distributions were obtained over an entire composition range, while the average diameters turned out to be very close to each other (1.5−2.3 nm). No aggregation of the bimetallic nanoclusters can be detected. Figure 1 shows a typical transmission electron micrograph and size distribution of Ni/Pd bimetallic nanoclusters with a mole ratio of Ni:Pd = 2:3 [abbreviated hereafter as Ni/Pd(2/3)]. The very small particles are considerably well-dispersed and uniform in size ranging from 1.2 to 2.5 nm with an average diameter of 1.9 nm (standard deviation $\sigma = 0.27$ nm). The TEM photographs of the particles with other composition ratios reveal the quite similar degree of dispersion. For the monometallic nickel system, probably due to the magnetic property of nickel,[20,21] the particles have a tendency to coagulate, although the particle size distribution remains quite narrow. In the monometallic palladium system, the particles display a wider size distribution and have a larger average diameter than those of the bimetallic cases, but still no aggregation is observed, which suggests the formation process or growth rate of palladium monometallic particles is different from the bimetallic particles.

Figure 2 shows the correlation between the average diameter and the standard deviation vs the metal composition of the nanocluster particles. For the clusters containing more than 30% of palladium, the average diameter gradually decreases as the mole ratio of the palladium decreases. The minimum average diameter (1.5 nm) was achieved for Ni/Pd bimetallic clusters with mole ratio of Ni:Pd = 7:3 clusters. The standard deviations are only in a range of 0.27−0.37 nm for the bimetallic clusters. The Ni/Pd(1/9) bimetallic clusters have the largest average diameter (2.3 nm) among the bimetallic nanoparticles, which is in close proximity to that of the monometallic Pd particle within expectation. Overall, the size distributions of the Ni/Pd bimetallic clusters do not show evident bimodal features, but appear in a notably narrow range. These facts strongly suggest that the colloidal dispersions of Ni/Pd bimetallic nanoclusters, thus obtained, are not mixtures of monometallic palladium and nickel nanoclusters, but consist of single particles having an "alloy" structure involving both palladium and nickel atoms in each particle. If alloy particles were not formed, there would be a broad or bimodal size distribution due to different growth rates for the two metal clusters, which may in turn be correlated to their surface charges or cohesive energies.[22] An additional

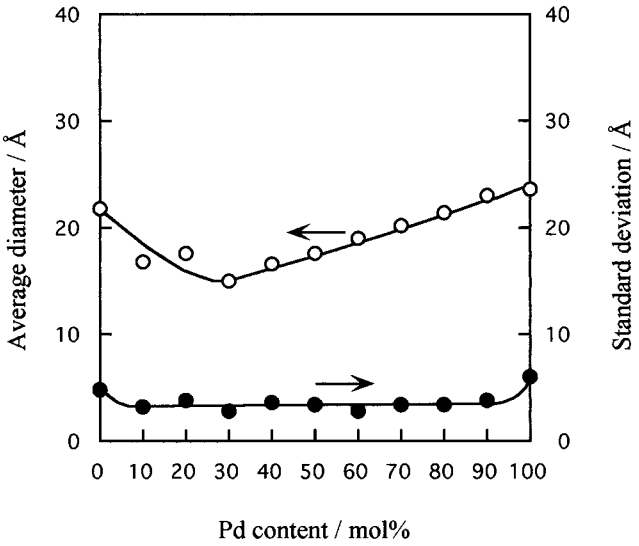

Figure 2. Plots of average diameter (open circle) and standard deviation (closed circle) of Ni/Pd bimetallic nanoclusters vs Ni/Pd ratio (*Y*-axis unit: Å).

experiment shows that a TEM photograph of a 1:1 mixture of monometallic nickel and palladium is very different from that of Ni/Pd bimetallic nanoclusters, as the mixture is composed of relatively larger particles and aggregation of smaller particles.

For further characterization of the alloy nanoclusters, their lattice images were observed by using high-resolution TEM (HRTEM). Crystalline palladium and nickel are known to have a face-centered cubic (fcc) structure, with (111) lattice distances of 0.2242 and 0.2030 nm, respectively.[23a] The crystalline structures of small metallic particles are sometimes the same as the bulk ones, but often different from the latter, showing lattice contractions or expansions.[23b] It is well established that the lattice parameters of many small metallic particles decrease with their sizes.[24] For example, lattice contraction with decreasing particle size has been reported for Cu, Ni, Ag, Au, and even Pd monoclusters.[24e,f] The interatomic distances of the nanometer-sized particles were found to be smaller than that of the bulk by 0.5−2% contraction. The lattice contraction can be explained using the theoretical treatment by Vermaak, Mays, and Kuhlmann-Wilsdorf.[24b] According to this work the observed lattice contraction can be interpreted in terms of a lattice stress. A contraction of the lattice parameter for small palladium particles prepared with a plasma polymer matrix from a vinyltrimethylsilane monomer has been reported.[24g] On the basis of the HRTEM measurements, the Pd nanoclusters prepared in the present study have a lattice spacing of 0.208 nm for the (111) plane, which is contracted by 7% with respect to the bulk. The resolving power of modern microscopy is sufficient to measure such small particles as the present nickel nanoclusters (∼2.2 nm), but the limitation could be caused by the contrast, especially for a comparatively low-Z element like nickel.[21] Probably due to this reason, as well as the usage of the larger amount of protective polymer in the case of nickel, a lattice parameter for nickel nanoclusters failed to be obtained from a very clear HRTEM image in the present investigation. We notice that Duteil, Schmid, and Meyer-Zaika have once carried out the HRTEM measurement, which shows that ligand-stabilized nickel particles dispersed in diethyl ether in the presence of PPh_3 have 19−21 (111) layers, corresponding to 3.9−4.3 nm diameters.[25]

It is well-known that Ni and Pd form a continuous fcc solid solution over the whole composition range for the case of bulk

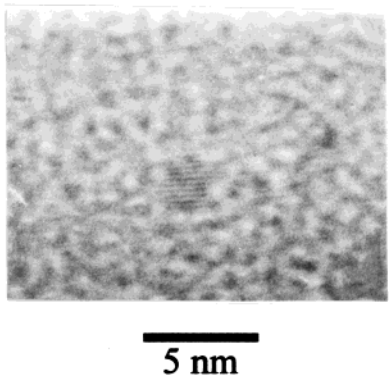

Figure 3. HRTEM photograph of Ni/Pd(1/4) nanoclusters.

metal.[23a,c] Figure 3 presents a representative HRTEM image of Ni/Pd(1/4) nanoclusters, showing a clear and well-ordered single-crystal lattice. The striped pattern in the particles indicates the (111) close-packing plane of the fcc structure. The lattice spacing has been measured to be 0.254 nm which is expanded by ∼15% compared with the corresponding bulk alloy (0.2215 nm).[23a,c] In the case of the Ni/Pd bimetallic nanoclusters with other intermediate composition ratios, there also exist the single-crystalline alloy structures with a uniform and dilated lattice spacing. Besides, lattice spacing decreases monotonically with the decrease of palladium content from 80 to 30 mol %, where the particle size also decreases systematically as shown in Figure 2. Only in Ni-rich nanoparticles (Pd% ≤ 20 mol %, like Ni/Pd(9/1) and Ni/Pd(4/1) clusters) or Pd-rich nanoclusters (Pd% = 90 mol %) two different values of lattice spacings are observed, corresponding to a rather enriched nickel phase or palladium phase. A similar phenomenon has also been observed, for example, in the Cu/Pd bimetallic clusters containing less than 15 mol % of palladium[26] and Pt/Cr alloy in Pt−Cr/HZSM-5 catalysts.[27]

To gain more insight into the alloy structure of Ni/Pd bimetallic nanoclusters, X-ray diffraction (XRD) of the dried dispersions was also carried out, and compared with that of Ni/Pd metal foils. The (111) lattice spacings of the Ni/Pd nanoclusters calculated from HRTEM and XRD measurements, respectively, are depicted in Figure 4 along with the values for bulk metals.[23a,c] The thin solid line represents theoretical Vegard's law, a linear relation of lattice constant based on the composition of alloy. Lattice spacing data from HRTEM measurements which correspond to the particles in the extreme minority or lack in enough reliability are parenthesized. It can be seen that the lattice parameter of Ni/Pd nanoclusters from XRD decreases almost linearly from 0.2283 nm for pure Pd particles to 0.2035 nm for pure Ni. Lattice parameters of Ni/Pd bulk metal from the literature vary from 0.2242 nm for pure Pd particles to 0.2030 nm for pure Ni with a small positive deviation from the theoretical Vegard's law. Similar phenomena can also be found in the systems such as Ni/Pt, Pd/Au, Pd/Ag, which may be related to the compressibility of the component metals.[28] A method to treat the pressure−volume relation in transition-metal alloys on the basis of virial theorem has been proposed by Kakehashi,[29] according to which the formation energy and the deviation of the lattice parameter from Vegard's law of Fe-base and Ni-base 3d transition metal alloys as well as Pd-base 4d transition metal alloys, were interpreted with three important factors, i.e., the d−d bonding effect, the s−d charge-transfer effect, and the magnetic effect due to the changes of the magnitudes of the local magnetic moments. Although the absolute lattice spacing values calculated from XRD and HRTEM are different due to the different levels of information

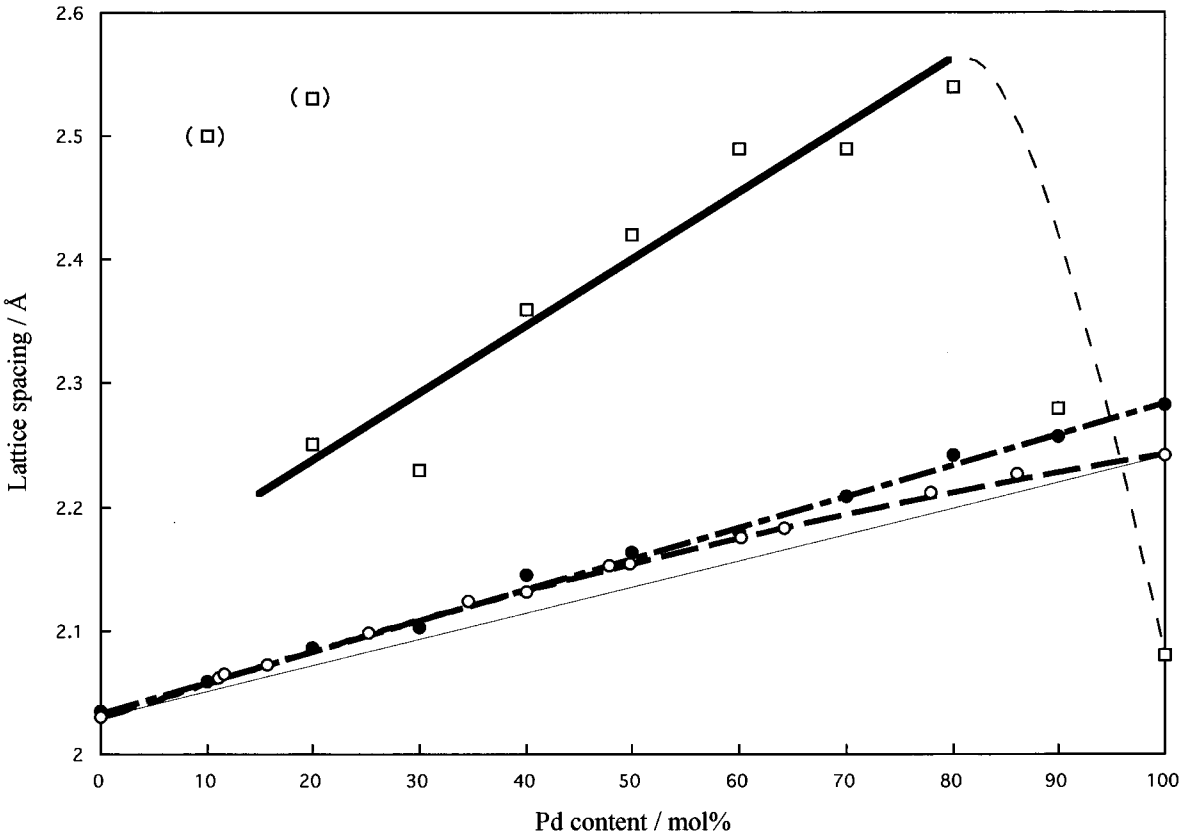

Figure 4. Plots of d(111) values calculated from HRTEM micrographs (thick solid line and open square) and XRD diffractograms (dot-and-dash line and closed circle) for Ni/Pd nanoclusters as well as the reference values for the Ni/Pd bulk alloy metals (thick dash curve and open circle) vs Ni/Pd ratio. The thin solid line represents theoretical Vegard's law behavior.

obtained by the two analytical techniques and the peculiarities of the two methods,[23b] it should be emphasized that both measurement results in the same changing tendency from pure Ni to pure Pd with regard to the alloy composition in the main intermediate composition range, which clearly reflects the alloy nature of the Ni/Pd particles. As for the phenomenon of the lattice deviation, we notice that there are some recent reports on the lattice parameter study of bimetallic alloy particles based on HRTEM measurement, which involve those of Cr/Pt,[27,30a] Ni/Sn,[30b] Ni/Pt,[30c,e] Cu/Ag,[30f] Sn/Pd,[30b] Sn/Pt,[30b] Ru/Pt,[30g,h] Ag/Pt,[22] Pd/Au,[30i] Ag/Au,[30d,f] and Pt/Au[30i] particles. An interesting and frequent finding is that many of the colloidal alloy particles under these studies show various levels of deviation of the lattice parameters from Vegard's law, either by contraction or dilatation, as well as more complications in their crystalline structures with respect to the bulk alloys. It is of note that Pearson carefully studied the structure determination and lattice spacings in the theory of alloy formation,[23b] and stressed that there are three main factors leading to lattice distortion: valency difference, relative size of solute and solvent atoms in a metal solid solution, and electrochemical differences. Pearson also pointed out the influence of particle size on lattice spacing and crystal structure, which may give an important concept for our results. Although the precise reason of the dilatation in the Ni/Pd nanocluster system under study is not clear yet, we have observed similar phenomena in Cu/Pd bimetallic nanoclusters also prepared by a polyol reduction method by HRTEM measurement.[26] One of the possible reasons to account for this interesting observation is the large number of surface atoms which are relaxed from their normal crystal lattice equilibrium positions by occlusion of extra elements.[24g,31] In addition, other factors, like the malleable nature of metals, may also promote the increase in the lattice parameters of the nanoclusters. Furthermore, incorporation of a minute amount of impurities such as carbon, hydrogen, hydroxyl group, or other byproducts in the preparation process into the Ni/Pd lattice may still be assumed as a plausible reason for the significant lattice expansion.[24g,32]

No X-ray diffraction line for pure Ni, Pd, or their oxides can be detected in the Ni/Pd nanoclusters, implying that nickel and palladium ions have been reduced to the zero-valence state under the present conditions. To ensure that the observed XRD patterns are not due to physical mixtures of Ni and Pd nanoparticles, we have compared the observed XRD patterns of the bimetallic particles with those of the corresponding mixtures. The XRD pattern of the mixture of Ni and Pd nanoparticles is composed of separate lines of Ni and Pd, while that of the Ni/Pd(1/1) bimetallic nanoclusters is composed of unique lines of the alloy between the lines of Ni and Pd. On the basis of this observation, it is further established that Ni/Pd bimetallic nanoclusters are composed of a Ni/Pd alloy phase rather than a mixed phase of monometallic nickel and palladium nanoclusters. In addition, the Ni/Pd nanoclusters exhibit a systematic change in the positions of the (111) reflections depending on the composition of Ni and Pd, suggesting the formation of Ni/Pd solid solutions.

X-ray photoelectron spectroscopy (XPS) of the dried samples was employed to determine the oxidation state of nickel in the PVP-protected Ni/Pd bimetallic nanoclusters. Nickel 2p electrons (Figure 5) had 2p3/2 and 2p1/2 binding energies of 852.6 and 869.5 eV, respectively. These binding energies are consistent with a metallic state of nickel, but lower than those of nickel oxides, for example, NiO or Ni_2O_3, respectively, indicating that nickel in the PVP-protected bimetallic nanoclusters is in the zero-valence state. Grim et al. reported that the binding energy for 2p3/2 band in Ni(0) metal powder is at 852.8 eV.[33] Tolman et al. investigated a variety of Ni(0) organometallic compounds and found that in zero-valence state Ni complexes, the Ni 2p3/2

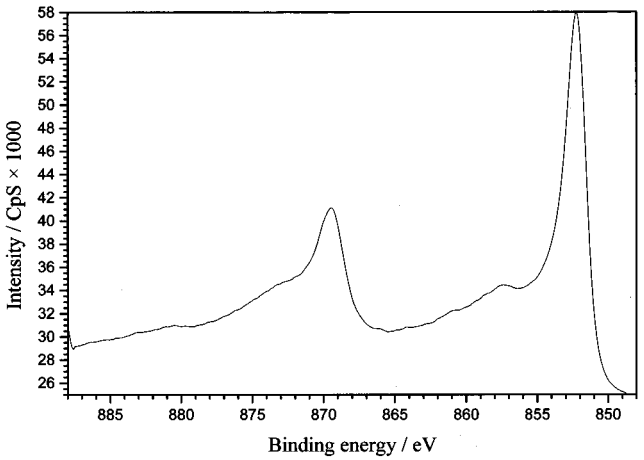

Figure 5. XPS spectra of Ni (2p) region in Ni/Pd(1/1) nanoclusters.

binding energies span a range of 853.6−856.0 eV, while higher binding energies are observed in a range of 855.0−857.2 eV in Ni(II) complexes, and even higher binding energies are observed for Ni(IV) compounds.[34] Depending on the electron withdrawing properties of the ligands, the electron density in the Ni may vary in the same oxidation state. Matienzo et al. also extensively studied a series of nickel compounds in all of the oxidation states by XPS.[35] In NiO, binding energy values of 854.0 and 872.0 eV were found for Ni2p3/2 and 2p1/2 peaks, respectively. Furthermore, in the case of NiO and tetrahedral Ni(II) compounds, obvious shake-up (satellite) peaks can be found in the region at about 6 eV higher than a normal Ni 2p3/2 or 2p1/2 band because such compounds are paramagnetic, whereas Ni(0) compounds and square-planar complexes of Ni(II) do not produce satellite peaks, because they are diamagnetic. Therefore, the Ni 2p bands in Figure 5, showing low binding energy values and essentially no satellite features, indicate that Ni exists mainly as 0 valence state inside Ni/Pd nanoclusters rather than NiO−Pd forms. Air-resistibility of Ni in these bimetalllic nanoclusters originates mainly from the stabilization effect of Pd, which might be attributed to a partial charge transfer from Ni to Pd in the alloy clusters, as has been noticed by Hlil et al.[36]

X-ray absorption fine structure (XAFS) is a powerful technique for characterization of structures and electronic states of nanoscopic materials.[37] Both extended X-ray absorption fine structure (EXAFS) and X-ray absorption near-edge structure (XANES) are crucial for the elucidation of the structural information, which is difficult, if not impossible, to obtain by other methods, especially for ultrafine alloy particles.[5−8,14,24h,38] Here, the results of XANES and EXAFS measured for Ni/Pd bimetallic nanoclusters are presented in order to confirm the structure.

The near-edge regions of X-ray absorption spectra can give direct information on the oxidation state of nickel, and these data have in fact been used in analyzing mixtures of nickel compounds of different oxidation states[39] or many Ni-containing bimetallic catalyst systems.[36,40] A selection of Ni K-edge XANES spectra of the Ni metal foil, and NiO and Ni_3O_4 powders are presented as the references with their first derivatives (as insets) in Figure 6a, b, and c. Both features A and B are attributed to the transitions from 1s to unoccupied final states originating from hybridized 4s, 4p, and 3d levels. These final states are described mainly as 3d character for feature A (quadrupole allowed, but dipole-forbidden 1s → 3d electronic transition) and s−p character for feature B (dipole-allowed 1s → 4p electron transition).[36,39a] It is widely recognized that feature A, which appears as a weak preedge peak at about 8330.0 eV in Figure 6a, b, is characteristic of Ni oxide compounds or Ni in oxidized states. Although the nickel XANES spectra of NiO and Ni_3O_4 in Figure 7a,b show a little difference, the variations are not so noticeable as the difference between oxides and metallic foil.

In Figure 6c, the feature A′, observed as a shoulder above the absorption rising edge and positioned at the corresponding preedge region from 8323 to 8335 eV, indicates the presence of Ni metal. Because of the different type of backscattering atoms in metal and oxides, it is inappropriate to compare the spectra of metallic Ni and the oxide in the preedge region. On the other hand, the half-height position of the main intense peak (feature B, also called "white line") is dependent on the oxidation state of Ni. It is very difficult to carry out the fitting of such spectra to determine the energies of distinct resonances and the absorption edge itself. Here we consider the corresponding inflection points given by the maxima in the first derivatives, since the features of the edge are more pronounced by comparing their derivative spectra.[24h] We observe significant differences in the energy positions and the intensities of both the preedge features and the rising edge of the white lines between the derivative spectra of the oxide and the metallic foil in Figure 6.

The XANES spectrum of Ni/Pd(4/1) bimetallic nanoclusters is shown in Figure 6d, which resembles that of Ni metal foil (Figure 6c) indicating the existence of zero-valent Ni. More precise discussion of the oxidation state can be carried out by using the first derivative of XANES spectra. For example, the first derivative of the XANES spectra shown in Figure 6a,b indicates peak maximum at 8335.5 and 8337.0 eV for the NiO and Ni_3O_4, respectively. Thus, the higher oxidation states are accompanied by the higher positions of the inflection points of feature B in the K-edge energies. If we compare the derivative spectrum of the Ni/Pd nanoclusters with that of Ni metal foil, then it also resembles that of Ni metal, with coincidence in the position of the maximum at 8329.0 eV, reflecting a close matching of the inflection points of the appropriate rising edges. This similar energy position of the absorption edge indicates the presence of Ni^0 in the nanoclusters. In addition, the shape of edge spectra of the alloy nanoclusters (Figure 6d) contrasts markedly to all the features of nickel oxides, indicating the absence of nickel in the oxidized state. Therefore, it is further established that Ni(II) ions have been reduced completely to the state of zero valence in the current cold alloying process. For the Ni/Pd colloids with other composition ratios, similar XANES spectra have been obtained; again, in these samples, it has been proved that Ni(II) ions have also been reduced completely to the state of zero valence by the close examination of their XANES spectra themselves and first derivative of XANES spectra. EXAFS analysis further supports this point. Fitting of theoretical and experimental EXAFS spectra becomes worse or impossible if the Ni−O bond is considered in calculation for Ni/Pd(4/1 and other ratios) alloy nanoclusters, which provides additional evidence for the absence of Ni−O bonds in the samples under study (vide infra).

For the purpose of investigating the air-resistance property of these novel Ni/Pd bimetallic nanocluster catalysts, we have measured XANES spectra of a series of Ni/Pd bimetallic nanoclusters with different composition ratios which have been kept stirring under oxygen flow at room temperature for three days after having been prepared under nitrogen. As a result, even after the oxygen treatment, the oxidation state of nickel, checked by XANES, almost remained at the zero valence state. Their XANES spectra showed that the dominating content of

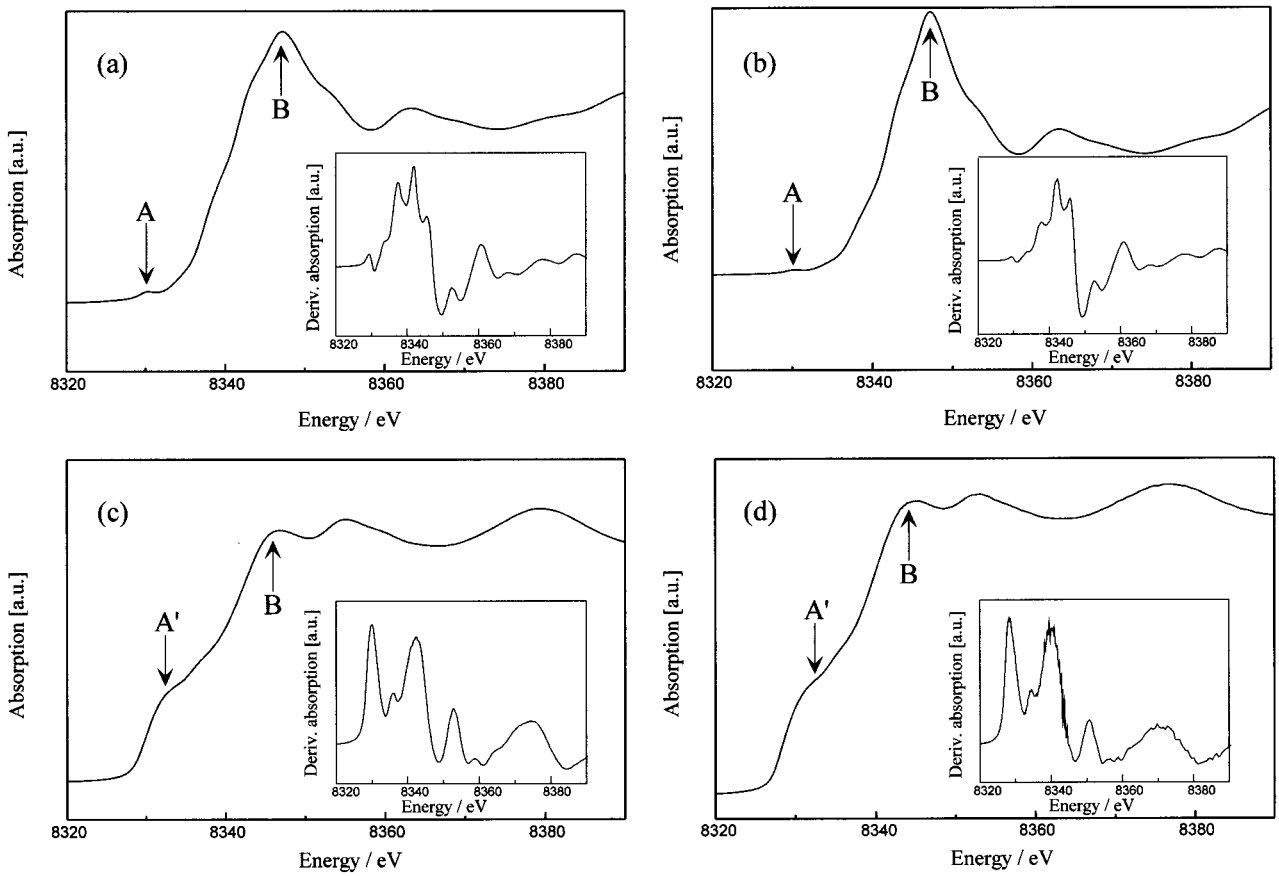

Figure 6. XANES spectra at the Ni K-edge and their first derivatives for (a) NiO, (b) Ni_3O_4, (c) metallic nickel foil, and (d) Ni/Pd(4/1) nanoclusters.

Ni is metallic, with only a minor part in an oxidized state. While the shape of feature B in the XANES spectra became a little sharper and somewhat like that of Ni oxides in some samples with high content of Ni, the shapes of the edge spectra as a whole were kept in close similarity with that of metallic nickel. Especially, the feature A′, observed still as a shoulder above the absorption rising edge and positioned at the corresponding preedge region from 8323 to 8335 eV, indicates the presence of Ni metal in the overwhelming majority. So, even after this kind of deliberate oxygen treatment, only minor, if any, oxidation has occurred. The only Ni atoms existing on the surface of the Ni/Pd colloids could possibly be the object of this kind of oxidation. Thus, it can be concluded that the Ni/Pd colloidal catalysts hold considerable air-resistance property originating from the stabilization effect of Pd and PVP, despite the common knowledge that Ni is very sensitive to oxygen.

To understand the detailed structure of PVP-protected Ni/Pd bimetallic nanoclusters, we have measured the EXAFS spectra of these nanoclusters as well as those of the corresponding metal and alloy foils at various Ni/Pd ratios. Figure 7a shows the k^3-weighted Fourier transformed EXAFS spectra at Ni K-edge of Ni foil and Ni/Pd alloy foils with different compositions 9/1, 1/1, and 1/9 in mole ratio. The main strong peak found in the spectrum of Ni foil should be attributed to the Ni−Ni metal bond, which was confirmed and determined to be 0.249 nm in distance by the curve-fitting analysis of the inverse Fourier transformed spectra. When the Ni/Pd ratio decreases, the above main peak gradually splits into two peaks, as in the case of Ni/Pd(1/1) foil. In the case of the Ni/Pd(1/9) foil, the main peak mentioned above decreases in height to form a weak shoulder peak and the other peak at a longer distance becomes the strongest. The newly appeared peaks at longer distances are mainly attributed to the Ni−Pd bond. It is clearly observed in Figure 7a that the original main peak due to Ni−Ni bond decreases its intensity with the increase of Pd content while the interference peak on the right increases its intensity.

Figure 7c shows the Fourier transformed EXAFS spectra at the Ni K-edge of the colloidal dispersions of Ni nanocluster and the Ni/Pd bimetallic nanoclusters with Ni/Pd mole ratios at 1/1, 2/3, and 1/4. The main peak for the Ni nanocluster should be assigned to the Ni−Ni metal bond. In a series of EXAFS spectra of Ni/Pd(1/1, 2/3, and 1/4) bimetallic nanoclusters, the main peak assigned to the Ni−Ni bond progressively decreases in height with decreasing Ni/Pd ratio, and splits into two peaks. This tendency is quite similar to the spectral change in the Ni/Pd foil as Figure 7a shows. The peak observed at the bimetallic nanocluster with high Pd content can be mainly attributed to a Ni−Pd bond although there is some contribution of the phase shift arising from the interference between Ni and Pd atoms. The successive intensification of the peak on the right side with the increase of Pd content just shows the gradual increment of Ni−Pd bonds in these nanoclusters. Similar changes in the EXAFS spectra have been found in our previous studies of Pd/Pt and Pt/Rh bimetallic nanoclusters.[5,8] These results demonstrate that both Ni−Ni and Ni−Pd bonds exist at the same time within each particle of Ni/Pd bimetallic nanoclusters, i.e., the formation of the alloy structure.

Figure 7b shows the comparison of the Fourier transformed EXAFS spectra at the Pd K-edge of Pd foil and Ni/Pd alloy foils with different compositions 1/9, 1/1, and 9/1 in mole ratio. The main peak for Pd foil can be assigned to the Pd−Pd bond, which is proved and determined to be 0.274 nm in distance by curve-fitting analysis. Although the peak-splitting phenomenon for Ni/Pd alloy foil with intermediate Ni/Pd ratio is not so severe as that at the Ni K-edge shown in Figure 7a, the main peak

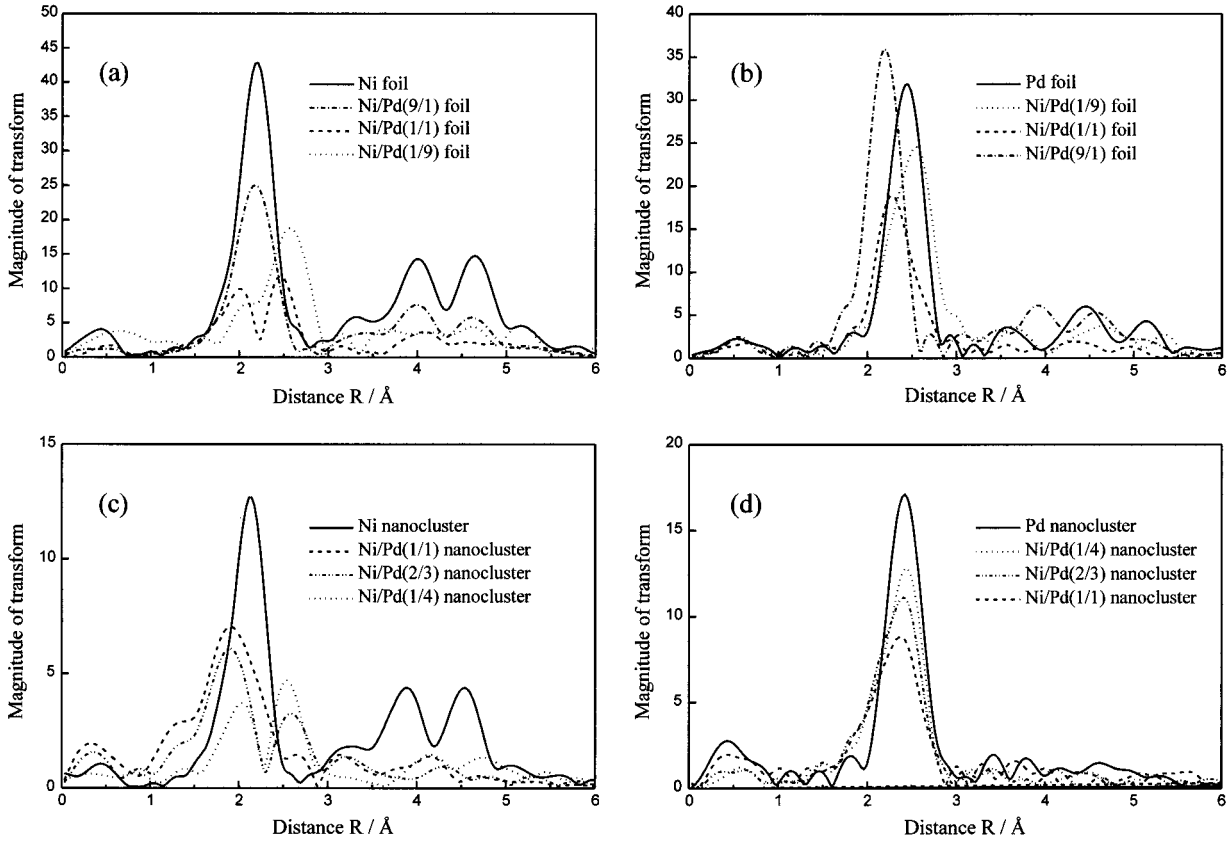

Figure 7. Fourier transformed EXAFS spectra (a) at the Ni K-edge of Ni foil, Ni/Pd(9/1) foil, Ni/Pd(1/1) foil, and Ni/Pd(1/9) foil, (b) at the Pd K-edge of Pd foil, Ni/Pd(1/9) foil, Ni/Pd(1/1) foil, and Ni/Pd(9/1) foil, (c) at the Ni K-edge of the colloidal dispersions of PVP-protected monometallic Ni nanoclusters and Ni/Pd bimetallic nanoclusters at Ni/Pd mole ratio = 1/1, 2/3, and 1/4, and (d) at the Pd K-edge of the colloidal dispersions of PVP-protected monometallic Pd nanoclusters and Ni/Pd bimetallic nanoclusters at Ni/Pd mole ratio = 1/4, 2/3, and 1/1.

tends to shift to the left side gradually in an analogous manner that can be expected for this case.

Fourier transformed EXAFS spectra at the Pd K-edge of the colloidal dispersions of Pd nanoclusters and Ni/Pd bimetallic nanoclusters with Ni/Pd ratios at 1/4, 2/3, and 1/1 are shown in Figure 7d. In the case of the Pd nanoclusters, the main peak is attributed to the Pd−Pd metal bond. Just like the corresponding foils' case (Figure 7b), the main peak gradually decreases and shifts to the shorter distance side as the Ni/Pd ratio increases, indicating the formation of Pd−Ni bonds in addition to Pd−Pd bonds. These results clearly indicate that these bimetallic nanoparticles contain both metal elements in a particle and have an alloy structure.

In addition, detailed curve-fitting analyses of EXAFS have shown the existence of only Ni−Ni, Pd−Pd, and Ni−Pd bonds in the various ratio Ni/Pd bimetallic nanoclusters. The Ni−O or Pd−O bond was not observed, indicating that there are no Ni−O or Pd−O species within these particles. We can assume from these spectra that the bimetallic clusters shown in Figure 7 may have a random alloy structure. In other words, enough Ni atoms are located in the surface of Ni/Pd bimetallic nanoclusters. The details of the structural analysis will be published elsewhere. The presence of the Ni atoms in the surface may provide some *ensemble* effect for the catalysis of the Ni/Pd bimetallic clusters.

Catalytic Properties of the Bimetallic Nanoclusters. Colloidal dispersions of Ni/Pd bimetallic nanoclusters, prepared by the improved polyol reduction method under high temperature, were applied to the catalysis for hydrogenation of nitrobenzene. During the reaction, the mixtures remained homogeneous without any precipitation.

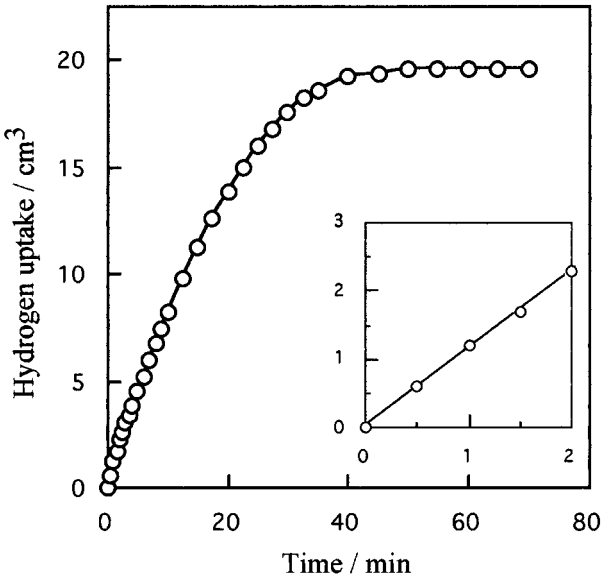

Figure 8. Hydrogen uptake vs reaction time in the hydrogenation of nitrobenzene catalyzed by a colloidal dispersion of Ni/Pd(1/1) bimetallic nanocluster. [nitrobenzene] = 14.3 mM, [Ni/Pd(1/1)] = 0.095 mM, solvent: ethanol, at 30 °C, $p(H_2) = 1$ atm. Inset shows the initial stage of the reaction on a magnified scale.

Figure 8 shows the temporal process of hydrogen uptake during the hydrogenation of nitrobenzene catalyzed by Ni/Pd-(1/1) nanoclusters. The hydrogen uptake, initiated immediately after addition of the substrate, increases linearly up to ca. 19.6 cm^3, where the hydrogen uptake suddenly ceased. The curve illustrates that the bimetallic nanoclusters have both high activity

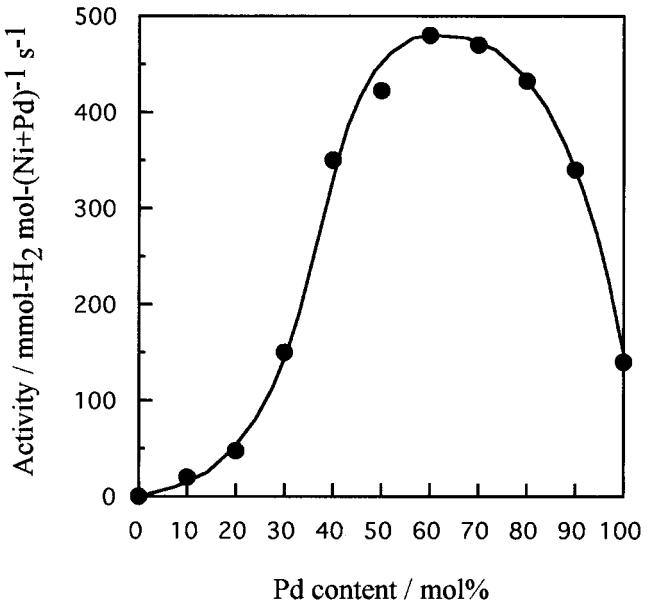

Figure 9. Relationship between the metal composition and the catalytic activity of the colloidal dispersions of Ni/Pd bimetallic nanoclusters for the hydrogenation of nitrobenzene.

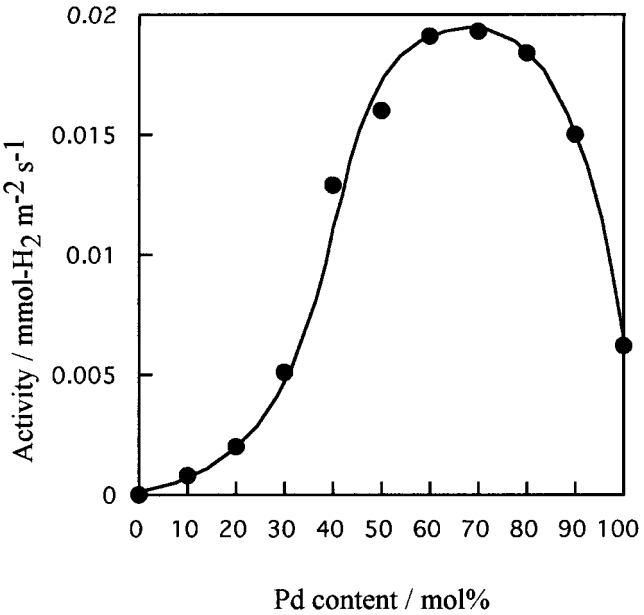

Figure 10. Relationship of catalytic activity, normalized by the surface area of the Ni/Pd bimetallic nanoclusters, vs Ni/Pd composition ratio. The original data were obtained from Figure 9.

and selectivity as a catalyst. In fact, product analyses by gas chromatography have proved that nitrobenzene has been stoichiometrically transformed to aniline, a reduction product, without any byproducts:

$$C_6H_5NO_2 + 3H_2 \xrightarrow{\text{Ni/Pd, 1 atm, 30 °C}} C_6H_5NH_2 + 2H_2O$$

Figure 9 shows the relationship between catalytic activity and the metal composition of bimetallic Ni/Pd nanoclusters during the hydrogenation of nitrobenzene. Palladium is known to be a good catalyst for the hydrogenation of nitro groups while nickel has very poor activity. Colloidal dispersions of bimetallic Ni/Pd nanoclusters have a considerably high activity. Ni/Pd nanoclusters containing Pd from 40 to 90 mol % show much higher activities than both Ni and Pd monometallic nanoclusters. In particular, Ni/Pd(2/3) clusters show the highest activity for nitrobenzene, ca. 3.5 times that of the monometallic Pd nanoclusters. Raney Ni, a typical Ni catalyst, was used for the hydrogenation of nitrobenzene under the same conditions as the present Ni/Pd bimetallic nanocluster catalyst for comparison. However, Raney Ni was proved to have no activity at all even though 5 times the amount of Ni was used. Similar situations were also observed for Pd black catalyst. In addition, mixtures of colloidal dispersions of monometallic palladium and nickel nanoclusters also exhibited quite low activity. This strongly corroborates that the bimetallic Ni/Pd nanoclusters, containing both palladium and nickel atoms in each particle, have a kind of an alloy structure, in which an *ensemble* interaction among palladium, nickel, and the substrate could enhance the catalytic activity.

To examine the effect of the surface area of the catalyst, the catalytic activity has been normalized by the surface area, which was calculated by using the average diameter of nanocluster particles measured by TEM. Dependence of the normalized activity on the metal composition (Figure 10) has the shape akin to that of the apparent activity (Figure 9). This indicates that the improvement in catalytic activity by the bimetallization is not due to increase in the surface area of particles. Other reasons such as ligand or *ensemble* effect in the bimetallic nanoclusters may account for this improvement.

As a result, palladium has a high catalytic activity, nickel has a low activity, while Ni/Pd bimetallic nanoclusters hold a catalytic activity higher than either of these monometallic nanoclusters for the hydrogenation of nitrobenzene. This result bears out the coexistence of both Pd and Ni atoms on the surface; i.e., the absence of a Pd shell on the nanocluster surface, which might be taken for granted to account for the good stability of Ni/Pd nanoclusters.

Meanwhile, some extent of surface segregation of palladium has also been suggested by EXAFS analysis. The total coordination number around nickel is found to be larger than that around palladium, suggesting that palladium atoms are located preferentially on the surface. So a model, where both elements are almost randomly distributed with a little enrichment of palladium near the surface, can be proposed for this novel light transition metal/noble metal bimetallic nanocluster. The adjacent palladium in this structure may assist the prevention of nickel from oxidation. In addition the neighboring nickel can provide an *ensemble* effect upon the catalysis of the palladium.

The catalytic activity of Ni/Pd bimetallic nanoclusters depends on the metal composition of the particle in the correlation shown in Figure 9. Polymer-protected Ni/Pd bimetallic nanoclusters in a certain intermediate composition range exhibit higher catalytic activity than either a nickel or palladium monometallic nanocluster, and at a certain Ni/Pd mole ratio, the maximum catalytic activity is observed. Although an exact reason for this interesting catalytic behavior of Ni/Pd bimetallic nanoclusters has not been verified yet, the following may be a possible interpretation. Two different kinds of effects of bimetallization may be predicted for the hydrogenation catalysis of nitrobenzene: (1) The increase of nickel on the surface may decrease the amount of palladium hydride (Pd−H) on the surface and consequently decrease the activity. (2) Since it is easier to form a charge-transfer complex with a benzene ring with nickel than with palladium, the increase of palladium on the surface may decrease the interaction between the substrate and the particle surface, and consequently decrease the activity. Thus, although the catalytic properties of an alloy cannot be deducted from the addition of the two metals forming it, coalescence of the above two effects may result in the present outcome.

4. Conclusions

Polymer-protected Ni/Pd bimetallic nanoclusters were obtained by an improved polyol reduction method under high temperature in the presence of poly(*N*-vinyl-2-pyrrolidone). TEM and HRTEM observations show that such nanoclusters have average diameters ranging from 1.5−2.3 nm, and that each metal particle contains Ni and Pd atoms in a relatively random arrangement. The HRTEM data also indicates an obvious deviation of lattice distance from Vegard's law, which may be due to a large number of surface atoms per particle. XRD, XPS, XANES, and EXAFS analyses have confirmed that the nickel in the bimetallic nanoclusters is in the zero-valence state, and that Ni and Pd atoms indeed form a random alloy. Rather random structure with a little deviation in distribution of each individual metal on the surface seems to be reasonable for the Ni/Pd bimetallic nanoclusters.

These novel bimetallic nanoclusters of light transition metal and noble metal was employed to catalyze the hydrogenation of nitrobenzene. They are proved to be an excellent catalyst with considerable air-resistance property for hydrogenation of nitrobenzene to aniline. Among the bimetallic nanoclusters with various Ni/Pd ratios a colloidal dispersion of Ni/Pd(2/3) nanoclusters has been found to be the most active catalyst. To conclude the discussion, the present results on polymer-protected Ni/Pd catalysts can offer a model of bimetallic nanocluster alloy catalyst system which is applicable over a wide range of metal dispersions.

Acknowledgment. The authors acknowledge Dr. Yukihide Shiraishi for his kind assistance in XPS measurement. This work has been supported by a Grant-in-Aid for Scientific Research in Priority Area "New Polymers and Their Nano-Organized System" (No. 08246101, to N.T.) from the Ministry of Education, Science, Sports and Culture, Japan.

References and Notes

(1) Toshima, N.; Yonezawa, T. *New J. Chem.* **1998**, 1179.

(2) Martens, J. H. A.; Prins, R.; Konningsberger, D. C. *J. Phys. Chem.* **1989**, *93*, 3179.

(3) Wunder, R. W.; Phillips, J. *J. Phys. Chem.* **1996**, *100*, 14430.

(4) Richard, D.; Couves, J. W.; Thomas, J. M. *Faraday Discuss. Chem. Soc*. **1991**, *92*, 109.

(5) Toshima, N.; Harada, M.; Yonezawa, T.; Kushihashi, K.; Asakura, K. *J. Phys. Chem.* **1991**, *95*, 7448.

(6) Toshima, N.; Harada, M.; Yamazaki, Y.; Asakura, K. *J. Phys. Chem.* **1992**, *96*, 9927.

(7) Harada, M.; Asakura, K.; Ueki, Y.; Toshima, N. *J. Phys. Chem*. **1993**, *97*, 10742.

(8) Harada, M.; Asakura, K.; Toshima, N. *J. Phys. Chem*. **1994**, *98*, 2653.

(9) Toshima, N.; Yonezawa, T.; Kushihashi, K. *J. Chem. Soc., Faraday Trans.* **1993**, *89*, 2537.

(10) Yonezawa, T.; Toshima, N. *J. Chem. Soc., Faraday Trans*. **1995**, *91*, 4111.

(11) Tong, Y. Y.; Yonezawa, T.; Toshima, N.; van der Klink, J. J. *J. Phys. Chem*. **1996**, *100*, 730.

(12) Wang, Y.; Toshima, N. *J. Phys. Chem*. *B* **1997**, *101*, 5301.

(13) Bradley, J. S.; Hill, E. W.; Klien, C.; Chaudret, B.; Duteil, A. *Chem. Mater*. **1993**, *5*, 254.

(14) Bradley, J. S.; Via, G. H.; Bonneviot, L.; Hill, E. W. *Chem. Mater*. **1996**, *8*, 1895.

(15) Toshima, N.; Wang, Y. *Langmuir* **1994**, *10*, 4575.

(16) Huang, H. H.; Yan, F. Q.; Kek, Y. M.; Chew, C. H.; Xu, G. Q.; Ji, W.; Oh, P. S.; Tang, S. H. *Langmuir* **1997**, *13*, 172.

(17) Nunomura, N.; Teranishi, T.; Miyake, M.; Oki, A.; Yamada, S.; Toshima, N.; Hori, H. *J. Magn. Magn. Mater*. **1998**, *177*, 947.

(18) Pizey, J. S. *Synthetic Regents*; Ellis Horwood Ltd.: Chichester, 1974; Vol. 2, pp 175−311.

(19) Chemical Society of Japan. *Kagaku Binran*; Maruzen: Tokyo, 1984; pp II−718.

(20) Reddy, B. V.; Nayak, S. K.; Khanna, S. N.; Rao, B. K.; Jena, P. *J Phys. Chem. A* **1998**, *102*, 1748.

(21) Gallezot, P.; Leclercq, C.; Fort, Y.; Caubère, P. *J. Mol. Catal.* **1994**, *93*, 79.

(22) Torigoe, K.; Nakajima, Y.; Esumi, K. *J. Phys. Chem.* **1993**, *97*, 8304.

(23) (a) Pearson, W. B. *Handbook of Lattice Spacings and Structures of Metals and Alloys*, Vol. 1 and 2; Pergamon Press: New York, 1967. (b) Pearson, W. B. *A Handbook of Lattice Spacings and Structures of Metals and Alloys;* Pergamon Press: Oxford, 1958; Chapter 3−5. (c) Massalski, T. B. *Binary Alloy Phase Diagrams*, 2nd ed., Vol. 3; The Materials Information Society: OH, 1989.

(24) (a) Berry, C. R. *Phys. Rev.* **1952**, *88*, 596. (b) Vermaak, J. S.; Mays, C. W.; Kuhlmann-Wilsdorf, D. *Surf. Sci.* **1968**, *12*, 128. (c) Solliard, C.; Flueli, M. *Surf. Sci.* **1985**, *156*, 487. (d) Montano, P. A.; Zhao, J.; Ramanathan, M.; Shenoy, G. K.; Schulze, W.; Urban, J. *Chem. Phys. Lett.* **1989**, *164*, 126. (e) Apai, G.; Hamilton, J. F.; Stohr, J.; Thompson, A. *Phys. Rev. Lett.* **1979**, *43*, 165. (f) Montano, P. A.; Shenoy, G. K.; Alp, E. E.; Schulze, W.; Urban, J. *Phys. Rev. Lett.*, **1986**, *56*, 2076. (g) Lamber, R.; Wetjen, S.; Jaeger, N. I. *Phys. Rev. B*, **1995**, *51*, 10968. (h) Franke, R.; Rothe, J.; Pollmann, J.; Hormes, J.; Bönnemann, H.; Brijoux, W.; Hindenburg, Th. *J. Am. Chem. Soc.* **1996**, *118*, 12090.

(25) Duteil, A.; Schmid, G.; Meyer-Zaika, W. *J. Chem. Soc., Chem. Commun.* **1995**, 31.

(26) Lu, P.; Dong, J.; Toshima, N. *Langmuir* **1999**, in press.

(27) Tkachenko, O. P.; Shpiro, E. S.; Jaeger, N. I.; Lamber, R.; Schulz-Ekloff, G.; Landmesser, H. *Catal. Lett.* **1994**, *23*, 251.

(28) (a) Allison, E. G.; Bond, G. C. *Catal. Rev.* **1972**, *7*, 233. (b) Domínguez, J. M.; Vazquez, A.; Renouprez, A. J.; José Yacamán, M. *J. Catal.* **1982**, *75*, 101.

(29) (a) Kakehashi, Y. *J. Phys. Soc. Jpn.* **1981**, *50*, 792. (b) Kakehashi, Y. *J. Phys. Soc. Jpn.* **1980**, *49*, 28.

(30) (a) Engels, S.; Lausch, H.; Peplinski, B,; Wilde, M.; Morke, W.; Kraak, P. *Appl. Catal.* **1989**, *55*, 93. (b) Arana, J.; de la Piscina, P. R.; Llorca, J.; Sales, J.; Homs, N.; Fierro, J. L. G. *Chem. Mater.* **1998**, *10*, 1333. (c) José Yacamán, M.; Fuentes, S.; Domínguez, J. M. *Surf. Sci.* **1981**, *106*, 472. (d) Link, S.; Wang, Z. L.; El-Sayed, M. A. *J. Phys. Chem. B* **1999**, *103*, 3529. (e) Bommannavar, A. S.; Montano, P. A.; Yacaman, M. J. *Surf. Sci.* **1985**, *156*, 426. (f) Itakura, T.; Torigoe, K.; Esumi, K. *Langmuir* **1995**, *11*, 4129. (g) Schmidt, T. J.; Noeske, M.; Gasteiger, H. A.; Behm, R. J.; Britz. P.; Bönnemann, H. *J. Electrochem. Soc.* **1998**, *145*, 925. (h) Vogel, W.; Britz, P.; Bönnemann, H.; Rothe, J.; Hormes, J. *J. Phys. Chem. B* **1997**, *101*, 11029. (i) Schmid, G.; Lehnert, A.; Malm, J.-O.; Bovin, J.-O. *Angew. Chem., Int. Ed. Engl.* **1991**, *30*, 874.

(31) Varga, P.; Schmid, M.; Hofer, W. *Surf. Rev. Lett.* **1996**, *3*, 1831.

(32) (a) Peisl, H. In *Hydrogen in Metals*; Alefeld, G., Völkl, G., Eds.; Springer: Berlin, 1978. (b) Tröger, L.; Hünnefeld, H.; Nunes, S.; Oehring, M.; Fritsch, D. *J. Phys. Chem. B* **1997**, *101*, 1279. (c) Lengeler, B. *Solid State Commun.* **1985**, *55*, 679.

(33) Grim, S. O.; Matienzo, L. J.; Swartz, W. E. *J. Am. Chem. Soc*. **1972**, *94*, 5116.

(34) Tolman, C. A.; Riggs, W. M.; Linn, W. J.; King, C. M.; Wendt, R. C. *Inorg. Chem*. **1973**, *12*, 2770.

(35) Matienzo, L. J.; Yin, L. I.; Grim, S. O.; Swartz, W. E. *Inorg. Chem.* **1973**, *12*, 2762.

(36) (a) Moraweck, B.; Renouprez, A. J.; Hlil, E. K.; Baudoing-Savois, R. *J. Phys. Chem*. **1993**, *97*, 4288. (b) Hlil, E. K.; Baudoing-Savois, R.; Moraweck, B.; Renouprez, A. J. *J. Phys. Chem.* **1996**, *100*, 3102.

(37) (a) Iwasawa, Y. *X-ray Absorption Fine Structure for Catalysts and Surfaces (World Scientific Series on Synchrotron Radiation Techniques and Applications*, Vol. 2); World Scientific: Singapore, 1996. (b) *X-ray Absorption: Techniques of EXAFS, SEXAFS and XANES*; Koningsberger, D. C., Prins, R., Eds.; J. Wiley & Sons: New York, 1988.

(38) (a) Sinfelt, J. H. *Acc. Chem. Res.* **1987**, *20*, 134. (b) Kolb, U.; Quaiser, S. A.; Winter, M.; Reetz, M. T. *Chem. Mater*. **1996**, *8*, 1889.

(39) (a) Mansour, A. N.; Melendres, C. A.; Pankuch, M.; Brizzolara, R. A. *J. Electrochem. Soc.* **1994**, *141*, L69. (b) Jentys, A.; Haller, G. L.; Lercher, J. A. *J. Phys. Chem.* **1993**, *97*, 484. (c) Jentys, A.; McHugh, B. J.; Haller, G. L.; Lercher, J. A. *J. Phys. Chem.* **1992**, *96*, 1324. (d) Kuzmin, A.; Purans, J.; Rodionov, A. *J. Phys.: Condens. Matter* **1997**, *9*, 6979. (e) Charnock, J. M.; Collison, D.; Garner, C. D.; McInnes, E. J. L.; Mosselmans, J. F. W.; Wilson, C. R. *J. Phys. IV France* **1997**, *7*, C2−657. (f) Jiménez-Ruiz, M.; Prieto, C.; Martínez, J. L.; Alonso, J. M. *J. Solid State Chem.* **1998**, *140*, 278.

(40) Hsieh, H. H.; Chang, Y. K.; Pong, W. F.; Pieh, J. Y.; Tseng, P. K.; Sham, T. K.; Coulthard, I.; Naftel, S. J.; Lee, J. F.; Chung, S. C.; Tsang, K. L. *Phys. Rev. B* **1998**, *57*, 15204.